



HAL
open science

Temporal Separation between Lattice Dynamics and Electronic Spin-State Switching in Spin-Crossover Thin Films Evidenced by Time-Resolved X-Ray Diffraction

Karl Ridier, Roman Bertoni, Ritwika Mandal, Alix Volte, Yifeng Jiang, Elzbieta Trzop, Matteo Levantino, Yves Watier, Johannes Frey, Yuteng Zhang, et al.

► To cite this version:

Karl Ridier, Roman Bertoni, Ritwika Mandal, Alix Volte, Yifeng Jiang, et al.. Temporal Separation between Lattice Dynamics and Electronic Spin-State Switching in Spin-Crossover Thin Films Evidenced by Time-Resolved X-Ray Diffraction. *Advanced Functional Materials*, 2024, 34 (41), pp.2403585. 10.1002/adfm.202403585 . hal-04649865

HAL Id: hal-04649865

<https://hal.science/hal-04649865v1>

Submitted on 22 Jul 2024

HAL is a multi-disciplinary open access archive for the deposit and dissemination of scientific research documents, whether they are published or not. The documents may come from teaching and research institutions in France or abroad, or from public or private research centers.

L'archive ouverte pluridisciplinaire **HAL**, est destinée au dépôt et à la diffusion de documents scientifiques de niveau recherche, publiés ou non, émanant des établissements d'enseignement et de recherche français ou étrangers, des laboratoires publics ou privés.



Distributed under a Creative Commons Attribution 4.0 International License

Temporal Separation between Lattice Dynamics and Electronic Spin-State Switching in Spin-Crossover Thin Films Evidenced by Time-Resolved X-Ray Diffraction

Karl Ridier,* Roman Bertoni,* Ritwika Mandal, Alix Volte, Yifeng Jiang, Elzbieta Trzop, Matteo Levantino, Yves Watier, Johannes Frey, Yuteng Zhang, Thomas Pezeril, Hervé Cailleau, Gábor Molnár, Azzedine Bousseksou, Maciej Lorenc, and Céline Mariette*

Spin-crossover (SCO) complexes have drawn significant attention for the possibility to photoswitch their electronic spin state on a sub-picosecond timescale at the molecular level. However, the multi-step mechanism of laser-pulse-induced switching in solid state is not yet fully understood. Here, time-resolved synchrotron X-ray diffraction is used to follow the dynamics of the crystal lattice in response to a picosecond laser excitation in nanometric thin films of the SCO complex $[\text{Fe}(\text{HB}(1,2,4\text{-triazol-1-yl})_3)_2]$. The observed structural dynamics unambiguously reveal a lattice expansion on the 100 picosecond timescale, which is temporally decoupled both from the ultrafast molecular photoswitching process (occurring within 100 fs) and from the delayed, thermo-elastic (Arrhenius-driven) conversion (taking place ≈ 10 ns). These time-separated dynamics are also manifested by the observation of damped acoustic oscillations in the time evolution of the lattice volume, whereas no such oscillations are observed in the electronic spin-state dynamics. Overall, these results suggest the existence of a universal behavior whereby the intramolecular energy barrier between low-spin and high-spin states acts as an intrinsic dynamical bottleneck in the out-of-equilibrium spin-state switching dynamics of SCO materials.

1. Introduction

Photoinduced phase transformations of solid-state materials, triggered by a short laser excitation, are known to involve dynamical processes, such as structural changes and electronic redistributions, which are intrinsically multi-scale in time and space. As an example, among these dynamical processes, while photoinduced electronic switching is quasi-instantaneous, typically occurring on the femtosecond timescale, it is noteworthy that macroscopic volume change of materials instead requires motions of atoms or molecules over long distances. These movements are triggered by laser-induced stress, either in the form of ultrafast lattice heating and/or in response to sudden electronic changes.^[1–6] The associated acoustic time needed to propagate the resulting strain and recover mechanical equilibrium within the sample, which is dictated by the speed

K. Ridier, Y. Zhang, G. Molnár, A. Bousseksou
Laboratoire de Chimie de Coordination
CNRS UPR 8241
Université de Toulouse
205 route de Narbonne, Toulouse F-31077, France
E-mail: karl.ridier@lcc-toulouse.fr

R. Bertoni, R. Mandal, E. Trzop, T. Pezeril, H. Cailleau, M. Lorenc
Univ. Rennes
CNRS
IPR (Institut de Physique de Rennes) – UMR 6251
Rennes F-35000, France
E-mail: roman.bertoni@univ-rennes.fr

A. Volte, M. Levantino, Y. Watier, J. Frey, C. Mariette
European Synchrotron Radiation Facility
71 avenue des Martyrs, Grenoble F-38000, France
E-mail: celine.mariette@esrf.fr

Y. Jiang
European XFEL
Holzkoppel 4, 22869 Schenefeld, Germany

 The ORCID identification number(s) for the author(s) of this article can be found under <https://doi.org/10.1002/adfm.202403585>

© 2024 The Author(s). Advanced Functional Materials published by Wiley-VCH GmbH. This is an open access article under the terms of the [Creative Commons Attribution](https://creativecommons.org/licenses/by/4.0/) License, which permits use, distribution and reproduction in any medium, provided the original work is properly cited.

DOI: 10.1002/adfm.202403585

of sound (typically of a few km s⁻¹), falls in the order of picoseconds for nanometer-sized crystals^[5] and nanoseconds (in a gross approximation) for micrometer-sized crystals.^[7] Photoinduced phase transitions may, in addition, be subject to local and/or macroscopic activation barriers, which can further slow down (thermodynamic) electronic redistributions and atomic rearrangements in molecular materials.^[8–10] To gain clear insights into these different processes and their dynamical limits, ultrafast time-resolved experiments are used to delineate the respective contributions of electronic, molecular, and lattice degrees of freedom.^[11–14] More specifically, it turns out to be essential to explore the possible interplay (coupling) that can exist between macroscopic structural deformations and the electronic state of molecules, with the aim to examine how such coupling can possibly promote or hinder the occurrence of cooperative (fast and efficient) macroscopic phase transformations.

Among (photo-)switchable molecular materials, spin-crossover (SCO) compounds, which can switch reversibly between their low-spin (LS) and high-spin (HS) electronic configurations, constitute a fascinating class of stimuli-responsive materials presenting volume change and cooperative phase transformation.^[15–17] In a previous study,^[18] the observation of a cooperative photo-response in an Fe³⁺ SCO complex, whose spin-state switching dynamics was found to be scaling with the crystallite size, has given rise to the suggestion of a direct coupling between macroscopic lattice deformations and the electronic spin state of molecules. However, recent experiments support a new scheme whereby the macroscopic volume expansion and spin-state switching are separated in time following ultrafast photoexcitation.^[8,10]

Here, we focus on the study of the out-of-equilibrium photoswitching dynamics in the Fe²⁺ molecular SCO compound [Fe(HB(1,2,4-triazol-1-yl)₃)₂] (**1**). Bulk crystals of **1** exhibit an abrupt, first-order spin transition above room temperature (≈60 °C) between the LS (*S* = 0) and HS (*S* = 2) states.^[19] Importantly, the spin transition in **1** is isostructural, as the compound remains in the same orthorhombic space group (*Pbca*) in both LS and HS states (CIF file CCDC No. 1534491 and No. 1534492 for the complex in the LS and HS state, respectively). Furthermore, as this molecular complex is sublimable, it can be deposited by vacuum thermal evaporation in the form of smooth, dense, nanocrystalline thin films in which the SCO properties are close to those encountered in the bulk material.^[20] Notably, a high degree of crystallinity of the as-deposited films can be reached through water vapor post-annealing, which leads to highly-oriented nanocrystalline layers composed of ≈50-nm-sized crystallites growing with the orthorhombic *c*-axis normal to the substrate surface.^[20,21] Crucially, these vacuum-deposited films also exhibit high stability and switching endurance (>10⁷ thermal switching events) upon repeated cycling.^[22] Overall, the morphological, structural, and spin-state switching characteristics of these films make them ideal playground for pump-probe photoswitching experiments. Especially, they present significant advantages when compared to previously studied SCO systems,^[10,18,23,24] since the studied thin-film samples here do not imply the presence of a polymer matrix which makes the interpretation of the photoinduced dynamics more straightforward. Furthermore, in contrast to previously studied Fe³⁺ SCO

compounds,^[10,18,23,24] thin films of **1** display a relatively large volume change upon the spin transition as compared to the ordinary thermal expansion (see below). This aspect turns out to be crucial to better analyze the effect of the volumic expansion arising from the sole spin-state switching.

A previous study of the spin-state photoswitching dynamics in films of **1** by femtosecond optical spectroscopy revealed the existence of a two-step dynamics in the temporal evolution of the fraction of photoinduced HS molecules.^[8] The initial (sub-picosecond) photoswitching process is followed by an additional conversion step, occurring on a timescale of tens of nanoseconds. The observed dependency of this delayed switching step on the sample temperature revealed its thermally activated nature governed by the intramolecular energy barrier between the LS and HS states.^[8] However, the question of the dynamics of the crystal lattice volume change during the photoswitching process still arises, while the extent to which such structural modifications may influence in return the transformation of the molecular spin state is still a matter of debate.

To address these fundamental questions, we report here a time-resolved X-ray diffraction (XRD) study of the photoswitching structural dynamics in nanometric thin films of **1** using synchrotron large-scale facility (ESRF). This work, coupled with previously reported optical spectroscopy measurements,^[8] allows to unveil a more complete sequence of the structural and electronic processes at work during the photoinduced transformation (from the molecular to the material scale) of SCO thin films triggered by an (ultra-)short optical excitation. From this set of data, it appears that lattice and electronic degrees of freedom behave with separate dynamics, in such nanometric films, up to a typical timescale of tens of nanoseconds. Prior to this delay, lattice heating and volume expansion are found to occur without any modification of the electronic spin state of molecules, trapped by the intramolecular energy barrier between the LS and HS states. On the other hand, after this delay, thermodynamic equilibration can finally occur between molecular spin state and lattice conformation (with expanded volume and elevated temperature), resulting in a second, thermo-elastic (Arrhenius-driven) switching step during which structural and electronic changes ultimately take place in concert. Through these observations, we demonstrate that the photo-transformation dynamics of SCO nanomaterials are intrinsically limited by the existence of local energy barriers, which impose a temporal bottleneck in the spin-state switching process.

2. Results and Discussion

2.1. Structural Properties of Single Crystals of **1**

To characterize the structural change upon the thermally induced SCO in compound **1**, temperature-dependent XRD measurements were first performed (at thermal equilibrium) on a single crystal, using a laboratory diffractometer (see Experimental Section). **Figure 1** displays the thermal evolution of the orthorhombic lattice parameters (*a*, *b*, and *c*) and unit-cell volume (*V*) upon heating and cooling the crystal between 10 and 120 °C. A sharp discontinuity of the unit-cell parameters and volume is observed at ≈60 °C, characterized by a narrow (less than 1-K-wide) thermal hysteresis loop, which signals the occurrence

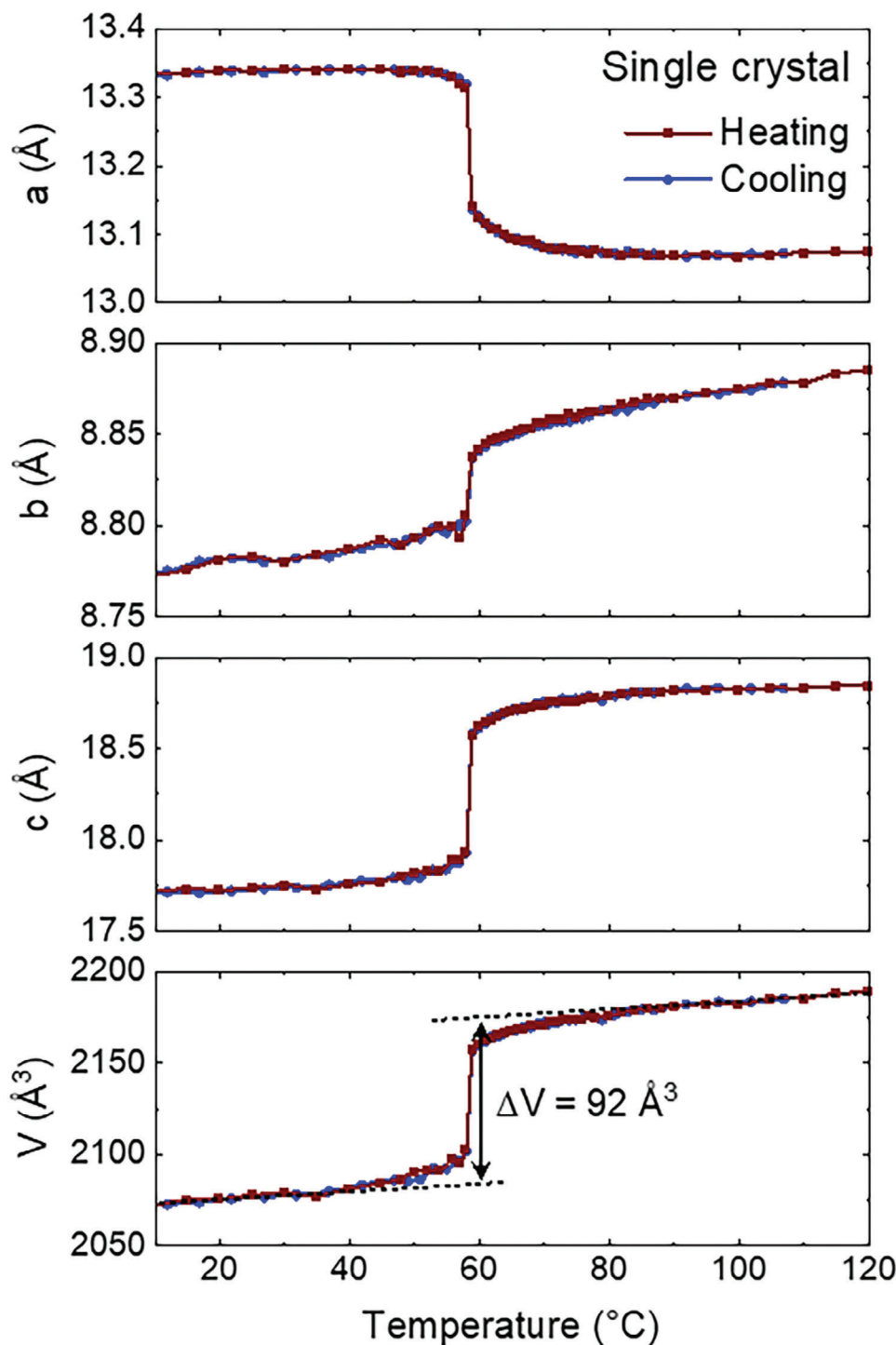


Figure 1. Thermal evolution of the orthorhombic lattice parameters (a , b , and c) and unit-cell volume (V) in a single crystal of **1**.

of a first-order spin transition as already reported previously via optical microscopy measurements.^[9,25] It is worth mentioning that the observed first-order transition does not occur between full LS and HS states since it was found to involve the switching of only $\approx 60\%$ of the molecules.^[9] As shown in Figure 1, in this SCO material, the unit-cell volume change accompanying

the complete LS-to-HS transition (excluding ordinary thermal expansion effects) is $\approx 92 \text{ \AA}^3$ (i.e., $\Delta V/V = 4.4\%$), which is consistent with the value previously reported using powder XRD.^[19] In Fe^{2+} SCO compounds, this sizeable volume expansion primarily arises from the large elongation of the Fe-N bond length of the coordination octahedron by ca. 0.18 \AA (i.e., $\approx 9\%$) upon the

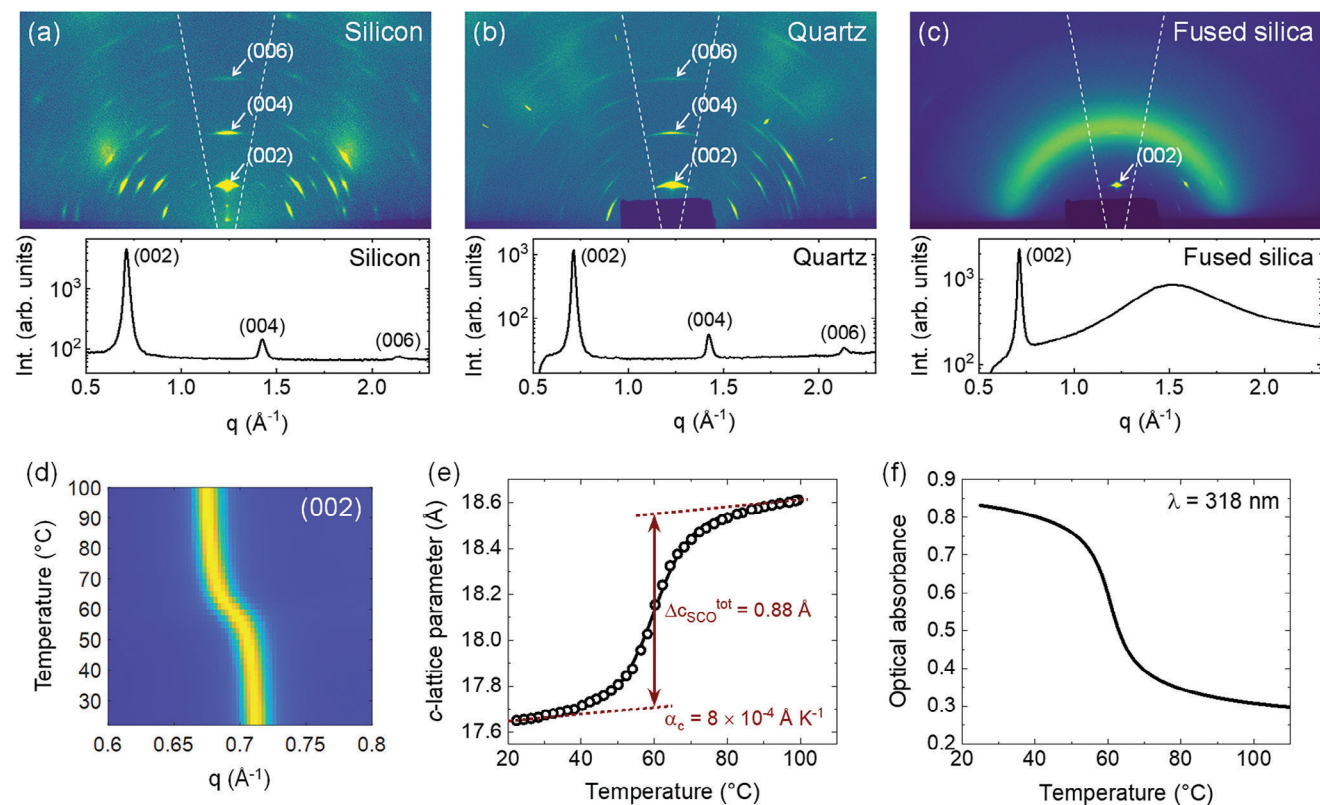


Figure 2. a) Synchrotron X-ray diffraction patterns, recorded at room temperature (LS state), of thin films of **1** deposited on a) silicon, b) single-crystal quartz, and c) amorphous fused-silica substrates. The thickness of the studied SCO films is 175 nm on silicon and fused silica and 210 nm on quartz. Below are the corresponding 1D diffraction patterns obtained after azimuthal averaging of the measured intensity on the diffraction images in the area delimited by the white dashed lines. d) Thermal evolution of the diffraction pattern of the 175-nm-thick film on fused silica, showing a clear shift of the (002) Bragg peak toward low q values upon the thermally induced LS-to-HS transition. e) Corresponding evolution of the c -lattice parameter in the film as a function of the temperature, compared to f) the thermal evolution of the optical absorbance ($\lambda = 318$ nm) measured on the same film.

LS-to-HS transition.^[26] Far from the spin-transition temperature, the volumic dilatation due to thermal expansion is found to be ca. $0.23 \text{ \AA}^3 \text{ K}^{-1}$ in both LS and HS states (corresponding to a thermal expansion coefficient of $1.1 \times 10^{-4} \text{ K}^{-1}$). As shown in Figure 1, the structural changes at the spin transition in **1** turn out to be strongly anisotropic. The data analysis reveals that the LS-to-HS transition is accompanied by a decrease of the a -lattice parameter, $\Delta a/a = -2.3\%$, while elongation is observed along the two other crystallographic axes, $\Delta b/b = 1.0\%$ and $\Delta c/c = 5.6\%$ (Figure 1). As a result, it appears that most of the unit-cell volume change originates from expansion/shrinkage of the c -lattice parameter, which thus constitutes one of the main structural fingerprints of the spin-state transition in compound **1**.

2.2. Structural Properties of Thin Films of **1** at Thermal Equilibrium

Temperature-dependent and time-resolved XRD measurements were performed on thin films of **1** at ESRF, ID09 beamline. As a first step, the structural signatures of the spin transition in the thin films were investigated at thermal equilibrium. XRD images were recorded on a 2D detector in quasi-grazing ($\theta = 1.5^{\circ}$) reflection geometry to reduce the scattering signal arising from

the substrate (see Experimental Section and Figure S1, Supporting Information for a schematic illustration of the experimental setup). Figure 2a–c show typical diffraction images of thin films of **1**, recorded at room temperature (LS state), deposited on silicon, single-crystal quartz, and amorphous fused-silica substrates, respectively. Regardless of the substrate used, it can be observed a preferred orientation of the crystallites with the c -axis normal to the substrate surface, while the a - and b -axes are randomly oriented in the plane (see Figure S2, Supporting Information for a schematic representation of the nanocrystalline structure of films of **1**). This leads to a reciprocal pattern with cylindrical symmetry, giving diffraction images with discrete signatures in reflection geometry (instead of diffraction rings).^[27] The angular width of these peaks allows us to estimate the angular distribution of the c -axis around the normal direction to be between 3 and 8 degrees depending on the film thickness. Due to the preferred orientation of the crystallites, the most intense Bragg peaks are located along the (00 l) direction, in which the diffracted intensity from all crystallites is concentrated in a single peak. Given the incidence angle (1.5°) of the beam, the X-ray energy bandwidth (1.5%), and the non-zero angular dispersion of the c -axis, the three Bragg peaks (002), (004), and (006) can be observed. More specifically, as depicted in Figure 2a–c (bottom panels), the 1D diffraction patterns obtained after azimuthal averaging of the diffraction intensity on

the 2D detector (in the area delimited by the dashed lines), reveal that the (002) Bragg peak (at a wavevector $q \approx 0.71 \text{ \AA}^{-1}$) is by far the most intense. Based on these results, in the following, we will thus mainly focus our analysis on the (00l) Bragg peaks, which exhibit the largest changes upon the SCO, with the aim to follow the lattice dynamics of the films through the evolution of the “SCO structural fingerprint” c -lattice parameter (vide supra).

As an example, Figure 2d displays the temperature evolution of the diffraction pattern recorded on a 175-nm-thick film of **1** on fused silica, across the thermally induced spin-state transition. These patterns reveal the occurrence of a notable shift of the (002) Bragg peak toward low q values, from $q = 0.712(1)$ to $0.675(1) \text{ \AA}^{-1}$, upon heating the film from 25 to 100 °C. The observed shift is particularly pronounced between 50 and 70 °C, demonstrating the substantial structural effect induced by the SCO phenomenon. From this shift of the (002) Bragg peak, Figure 2e shows the evolution of the c -lattice parameter in the film as a function of temperature (see Experimental Section). Note that since the crystallites are preferentially aligned with the c -axis normal to the film surface, as discussed above, this evolution of the c -parameter also reflects the thermally induced change of the film thickness. Interestingly, one can notice that the thermal evolution of the c -lattice parameter follows the same evolution as the UV optical absorbance (Figure 2f), indicating a direct correlation between the volume (thickness) change and the electronic spin state of molecules at thermal equilibrium. In addition to the peak shift, it is interesting to note that the transition is also accompanied by a measurable broadening of the (002) Bragg peak, which occurs in the same temperature range (50–70 °C), reaching a maximum value at the spin-transition temperature $T_{SCO} \approx 60 \text{ °C}$ (Figure S3, Supporting Information). Such a broadening of the diffraction peak signals the emergence of structural inhomogeneities in the thin-film sample during the spin-transition process, presumably because a large number of SCO crystallites is probed by the X-ray beam, which may exhibit slightly different transition properties depending on their size or due to the presence of local defects/strain within the film.^[28] Overall, these measurements indicate that the thermally induced spin transition in films of **1** occurs at a temperature range similar to that observed in bulk single crystals (Figure 1). However, the phase transition loses first-order character (no discontinuity is observed in the volume change), even though it remains relatively abrupt in temperature. A fit of the experimental data using a sigmoidal function (Figure 2e) allows to extract a linear dilatation in the film along the c -axis due to thermal expansion of $\alpha_c \approx 8 \times 10^{-4} \text{ \AA K}^{-1}$ in both spin states, while the change of the lattice parameter due to the sole spin-state transition is found to be $\Delta c_{SCO}^{tot} = 0.88 \text{ \AA}$, corresponding to a relative variation of $\Delta c_{SCO}^{tot}/c \approx 5.0\%$. Note that this relative change is lower than the one observed in single crystals ($\Delta c/c = 5.6\%$, Figure 1) probably due to the presence of grain boundaries in the film, which contribute to reducing a part of the volume change, or possibly due to a clamping effect of the substrate that may impede to some extent elongation/contraction along the substrate plane but also along the c -direction due to dynamical Poisson effect.^[29] Overall, this analysis indicates that thermal expansion effects in films of **1** remain relatively small compared to the lattice volume change induced by the sole spin-state transition. By way of comparison, the SCO phenomenon generates a total lattice elongation along the c -axis that should be equivalent

to the one produced by a temperature jump of $\approx 1100 \text{ °C}$ if only due to ordinary thermal expansion.

2.3. Time-Resolved Study of Thin Films

Afterward, time-resolved pump-probe XRD measurements were performed at ESRF, ID09 beamline. Thin films of **1** were photoexcited using a picosecond pump laser at $\lambda = 535 \text{ nm}$ (pulse duration 1.5 ps), wherein complex **1** in the LS state exhibits a weak ligand-field ($d-d$) transition associated with an absorption coefficient of $\alpha_{535 \text{ nm}} \approx 200 \text{ cm}^{-1}$.^[9] This low absorption coefficient implies a large laser penetration depth ($\delta \approx 50 \text{ }\mu\text{m}$) compared with the thickness ($L = 175\text{--}210 \text{ nm}$) of the studied films, thus ensuring a uniform distribution of photo-converted molecules and a homogeneous transient heating within the film thickness. The energy density of the pump laser was varied up to a maximum value of 26 mJ cm^{-2} , similar to that used in our previous study^[8] allowing for a direct comparison. It is worth mentioning that, considering the relatively low optical absorption at this wavelength, these photoexcitation conditions allow to remain in the single-photon excitation regime and do not induce nonlinear optical effects. The repetition rate of the experiment was set to 1 kHz and the temporal resolution, limited by the X-ray pulse duration, translates into an instrument response function of $\sim 70 \text{ ps}$. More details are provided in the Experimental Section. As an example, Figure 3a shows diffraction patterns of the 175-nm-thick film of **1** deposited on fused-silica substrate, displaying the evolution of the (002) Bragg peak at $T = 40 \text{ °C}$ at different time delays (covering 7 decades in time, from 100 ps to 1 ms) following a pulsed laser excitation of $I = 26 \text{ mJ cm}^{-2}$. The corresponding differential patterns (Figure 3a, bottom panel) reveal a shift of the (002) Bragg peak toward low q values at positive delays, meaning a photoinduced lengthening of the c -lattice parameter after irradiation. Based on this observed peak shift, the temporal evolution of the c -parameter expansion, Δc , can be monitored at $T = 40 \text{ °C}$ (see Figure 3b) in response to laser excitations of different energy densities. By comparison, Figure 3c shows the time evolution of the fraction of photoinduced HS molecules, Δn_{HS} , recorded through ultrafast optical spectroscopy^[8] on a thin film of **1** of similar thickness under comparable experimental conditions.

This direct comparison of the electronic and structural out-of-equilibrium dynamics in these nanometric thin films turns out to be extremely instructive. At first, as revealed by optical spectroscopy (Figure 3c) and reported in numerous studies,^[23,30] the pulsed laser excitation optically induces the conversion of a small fraction (typically few percent) of molecules, Δn_{HS}^{hv} , from the LS to the HS state within a few hundred femtoseconds (through an intersystem crossing process).^[31–34] In thin films of **1**, this fraction of photoinduced HS molecules remains constant up to a delay of a few nanoseconds, after which Δn_{HS} undergoes a second increase (for sufficiently high laser energy densities) to reach a peak value at $\approx 20\text{--}30 \text{ ns}$.^[8] This multi-step dynamics is followed by a relaxation into the initial LS state around the microsecond timescale. In parallel, time-resolved XRD data (Figure 3b) reveal that the change of the c -lattice parameter in the film takes place within the first 100 ps following laser excitation (whatever the laser energy density). Then, as for Δn_{HS} , Δc follows a plateau

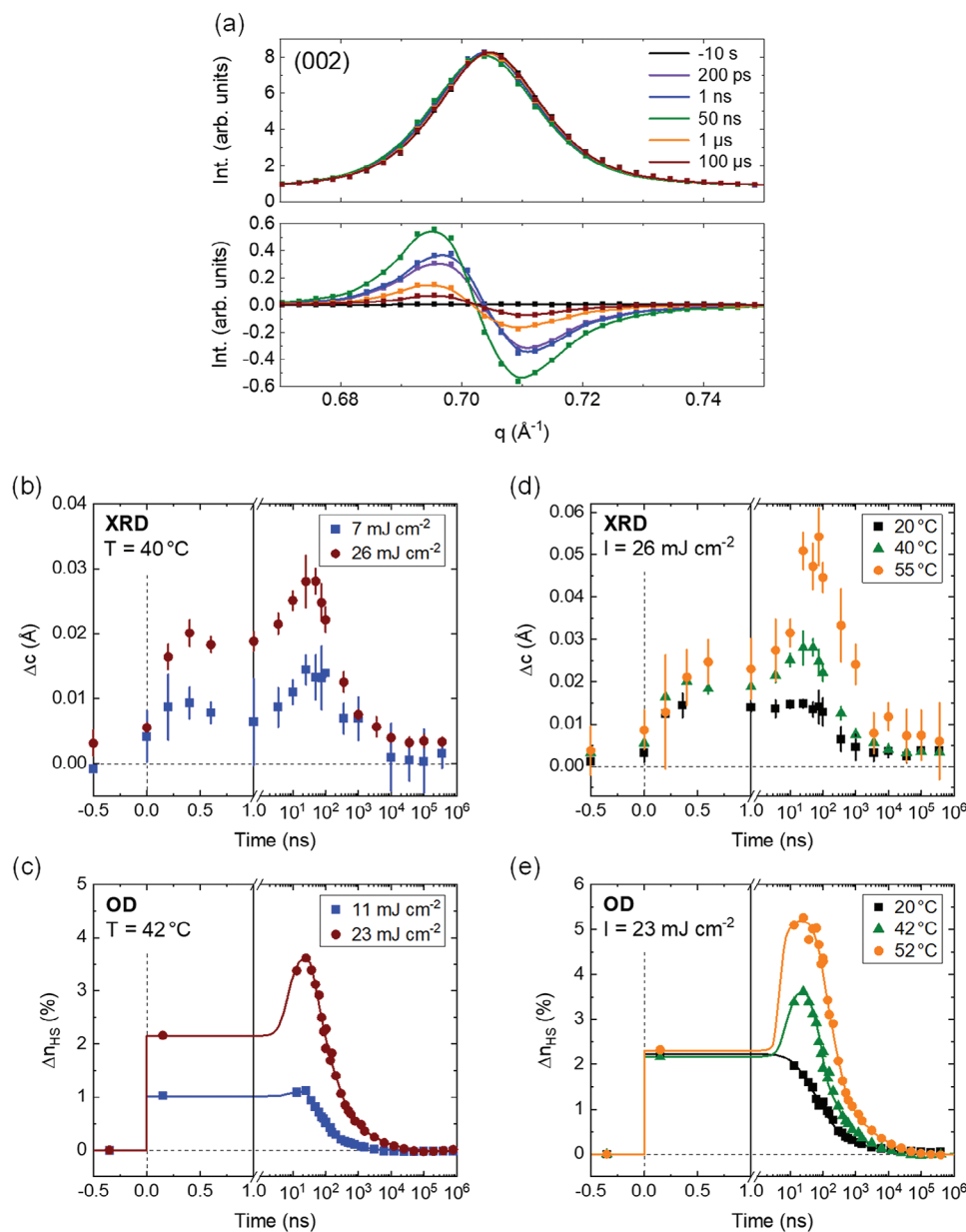


Figure 3. a) Time-resolved diffraction patterns showing the evolution of the (002) Bragg peak at different delays after picosecond laser excitation ($I = 26$ mJ cm^{-2}) at $T = 40$ $^{\circ}\text{C}$ of a 175-nm-thick film of **1** deposited on a fused-silica substrate. The solid lines are the result of a fit using a pseudo Voigt function. The curves below depict the corresponding difference patterns (obtained by considering the “laser OFF” diffraction patterns as a reference). b,d) Time evolution of Δc in the same film following (b) a laser pulse with two different energy densities at $T = 40$ $^{\circ}\text{C}$ and d) a laser pulse with an energy density of $I = 26$ mJ cm^{-2} at selected temperatures. c,e) Time evolution of the fraction of photoswitched HS molecules, Δn_{HS} , determined from optical spectroscopy measurements performed on a thin film of **1** of similar thickness (150 nm), adapted from ref. [8], following (c) a laser pulse with various energy densities at $T = 42$ $^{\circ}\text{C}$ and (e) a laser pulse with an energy density of $I = 23$ mJ cm^{-2} at selected temperatures.

until a time delay of a few nanoseconds, after which the crystal lattice volume undergoes a second increase to reach a maximum value at ≈ 20 – 30 ns, before returning to its initial value on the microsecond timescale.

This structural expansion observed on the 100 ps timescale originates from the generation of photoinduced stresses within the SCO film due to two distinct effects: i) the rearrangement and volume swelling of the photoswitched molecules and ii) the transient increase of the lattice temperature. The latter is known to

occur around tens of picoseconds,^[10,35,36] as a large part of the absorbed photon energy is transferred to the lattice.^[37,38] In response to these photoinduced stresses, the recovery of mechanical equilibrium with the external environment is achieved via the propagation of acoustic strain waves (collective motion of atoms), resulting in a lattice expansion.^[7,11,30] This lattice expansion is therefore expected to occur on the so-called acoustic timescale, which can be estimated to be around $\tau_{\text{ac}} = L/v \approx 60$ – 70 ps for the SCO film studied here, where L is the film thickness and

$v \approx 3000 \text{ m s}^{-1}$ is the longitudinal sound velocity in the SCO material (see below). This rough estimation matches our experimental time-resolved XRD observations. At the highest excitation energy density (26 mJ cm^{-2}), the initial fraction of photoinduced HS molecules reaches $\Delta n_{\text{HS}}^{hv} \approx 2\%$ (see Figure 3c), implying, if one takes into account the specific heat capacity of the material ($C_p = 1107 \text{ J kg}^{-1} \text{ K}^{-1}$),^[39] an overall increase of temperature estimated to be around $\Delta T \approx 6 \text{ K}$. Thus, an elementary calculation predicts an increase of the *c*-lattice parameter of $\Delta c_{\text{SCO}} = \Delta n_{\text{HS}}^{hv} \times \Delta c_{\text{SCO}}^{\text{tot}} \approx 0.017 \text{ \AA}$ due to the fraction of photoswitched molecules, and of $\Delta c_{\text{th}} = \Delta T \times \alpha_c \approx 0.005 \text{ \AA}$ due to the global temperature rise, giving an overall expansion equal to $\Delta c = \Delta c_{\text{SCO}} + \Delta c_{\text{th}} \approx 0.022 \text{ \AA}$, close to the value observed experimentally (Figure 3b). We can therefore presume that the lattice volume change observed on the 100 ps timescale may primarily arise from the photoinduced LS-to-HS molecular switching while only a minor contribution should originate from lattice heating. It is also worth mentioning that a non-zero baseline in Δc (at negative and long times) progressively arises for increasing laser excitation densities, most likely due to a stationary residual temperature rise of the sample in the present experimental conditions ($< 4 \text{ }^\circ\text{C}$ at 1 kHz repetition rate).

Another important result highlighted through the combination of structural and optical data (Figure 3b,c) is that on the time window spanning from 100 ps to a few nanoseconds, neither the lattice temperature rise nor the volume expansion of the film (hereafter referred to as thermo-elastic phenomena) triggers any immediate feedback on the electronic spin state of molecules. Indeed, as observed by optical spectroscopy,^[8] the fraction of photoinduced HS molecules remains constant up to the nanosecond timescale (see below) despite lattice temperature jump and volume expansion. An additional conversion of molecules into the HS state is only observed after $\approx 10 \text{ ns}$ following the laser excitation. This delay stems from the existence of a local LS \leftrightarrow HS intramolecular energy barrier, which governs the thermally activated conversion rate between the LS and HS states, shifting the molecular spin-state switching dynamics on a timescale of tens of nanoseconds.^[8] After this delay, the fraction of LS/HS molecules equilibrates with the new lattice conformation (volume and temperature), resulting in a second “thermo-elastic” switching step.^[8,10,18,24,40] Predictably, we observe that this additional conversion step is accompanied by a substantial volume expansion of the crystal lattice on the same timescale (Figure 3b). At high excitation density, optical measurements (Figure 3c) indicate a maximum additional increase of the HS fraction equal to $\Delta n_{\text{HS}}^{\text{th}} \approx 1.3\%$, which should correspond to an additional expansion along the *c*-axis of $\Delta c = \Delta n_{\text{HS}}^{\text{th}} \times \Delta c_{\text{SCO}}^{\text{tot}} \approx 0.01 \text{ \AA}$. This expected value is fully consistent with our XRD data. On the other hand, at low excitation density, no additional step is observed in terms of HS fraction and lattice expansion, because, in this case, the small amount of heat is evacuated out of the sample quick enough, preventing the further conversion of molecules into the HS state. Finally, due to heat diffusion and dissipation between the SCO film and the external environment, the (structural and electronic) relaxation back to the LS ground state is completed within $1 \mu\text{s}$ under the present experimental conditions.

In addition to the lattice expansion along the *c*-axis normal to the SCO film surface, it is worth mentioning that in-plane distortion should also occur, although a much smaller effect is expected

(Figure 1). Within our experiment geometry and resolution, no measurable in-plane distortion could be detected. However, further investigations would be needed to scrutinize whether in-plane expansion might play a role (even minor) in the delayed structural changes observed on the nanosecond timescale.^[41] Besides the lattice parameter changes, it should be also noted that a measurable broadening of the (002) Bragg peak is observed during the photoswitching process (Figure S3, Supporting Information). Similar to the peak shift, the width passes through a maximum $\approx 20\text{--}50 \text{ ns}$ after laser excitation (thermo-elastic step) signaling the occurrence of spin-state transition, as observed during the thermally induced SCO.

Temperature-dependent measurements were also carried out at a fixed excitation density (Figure 3d,e). As the fraction of photoinduced molecules and lattice heating are independent of the initial temperature (as long as the initial fraction of LS molecules remains identical), the magnitude of the lattice expansion on the acoustic timescale is seen to remain virtually unchanged independently of the investigated temperature (Figure 3d). However, a strong temperature dependence is observed for the thermo-elastic step occurring after 10 ns. Indeed, as the base temperature of the film approaches the transition temperature ($T_{\text{SCO}} \approx 60 \text{ }^\circ\text{C}$), the observed peak values of Δn_{HS} and Δc increase, because the heat generated by the laser pulse allows the thermally activated conversion of larger fractions of molecules. Noticeably, it appears that the peak of Δc observed at 20–30 ns seamlessly follows the evolution of the LS-to-HS thermo-elastic conversion step, indicating that, at this timescale, all internal degrees of freedom (electronic, molecular, and lattice) of the system have equilibrated.

Time-resolved XRD measurements were also carried out with finer time sampling to thoroughly probe the structural dynamics of the photoexcited films at short timescale ($< 700 \text{ ps}$). As shown in Figure 4a, the main observation is that the *c*-lattice parameter exhibits damped oscillations before reaching the plateau value. Such oscillations are repeatedly and reproducibly observed for different thin films of **1** on fused silica and other substrates. Independently of the substrate at use, Δc is found to reach a maximum value at a time delay of ca. 100 ps, before oscillating with a period of $236 \pm 10 \text{ ps}$. The origin of these oscillations can be explained by the fact that the internal stress, generated by lattice heating and molecular volume swelling, builds up faster than the lattice can expand over its macroscopic dimensions, i.e., faster than the time required for travelling strain waves to release the excess mechanical energy. The oscillations of the lattice volume indicate that this quasi-instantaneous stress gives rise to perfectly balanced strains, a static strain, and a propagating strain of opposite sign. The “overshoot” observed on the XRD data at $\approx 100 \text{ ps}$, which corresponds to the back-and-forth travel time ($2L/v$) of the propagating strain across the SCO film, illustrates the first constructive interference of the static strain with the propagating strain. Subsequent constructive interferences of the strains occur at round trip times in the film, generating this “breathing” acoustic effect of the SCO layer. Such oscillations are sometimes referred to as acoustic eigenmodes^[4,42–46] when the sample is homogeneously excited (no strain gradient within the thickness). Finally, it is only once the propagating strain completely vanishes into the substrate that the static strain fully arises, revealing a new mechanical equilibrium state on the nanosecond timescale. As shown in Figure 4b, which displays the evolution of the averaged

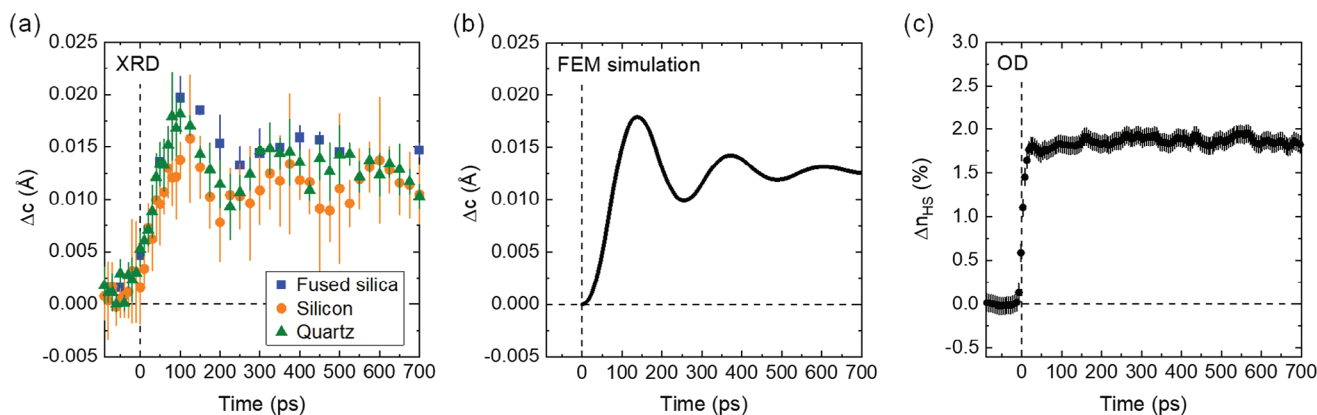


Figure 4. a) Time evolution of the orthorhombic c -lattice parameter of thin films of **1** deposited on various substrates, at room temperature, following a laser excitation of energy density $I = 26 \text{ mJ cm}^{-2}$. The film thicknesses are 175 nm for fused silica and silicon and 210 nm for quartz. The instrument response function of the time-resolved XRD setup can be approximated by a Gaussian function with 70-ps FWHM. b) Time-domain finite elements simulations of strain wave propagation in a film of **1** on a quartz substrate, allowing the observed oscillations of Δc to be reproduced on the sub-nanosecond timescale. c) Time evolution of the fraction of photoswitched HS molecules, Δn_{HS} , determined from optical spectroscopy measurements on a thin film of **1** of similar thickness (150 nm) under comparable experimental conditions ($T = 20 \text{ }^\circ\text{C}$, $I = 23 \text{ mJ cm}^{-2}$) (adapted from ref. [8]). No oscillations are observed in the dynamics of the photoinduced HS fraction.

strain over the entire film (static and propagating combined), it was possible to qualitatively reproduce the observed results by means of time-domain finite elements simulations (FEM), taking into account the 70-ps FWHM Gaussian instrument response function of the XRD setup. These FEM simulations were performed with the k -wave toolbox, in a similar manner to ref. [47], by assuming an instantaneous and uniform pressure jump over the whole SCO film thickness induced by the laser excitation. Details on the input parameters, such as the speed of sound, the density of the different materials, the film thickness, the input stress, the time, and spatial resolution, can be found in the video in the Supporting Information. The main characteristics of the “breathing” oscillations of Δc are well reproduced considering a longitudinal speed of sound of $v = 3000 \text{ m s}^{-1}$ in the SCO material. Given the similar acoustic impedance mismatch between the different substrates holding the films, the simulations did not show any pronounced effect on the nature of the substrate, as observed experimentally.

Overall, the present observations and simulations provide further evidence of a temporal separation between lattice and electronic spin-state dynamics in SCO nanometric thin films on the sub-nanosecond timescale. Indeed, while Δc undergoes damped oscillations, signaling the propagation of strain waves into the excited lattice, no oscillation of the HS fraction is concomitantly observed, as revealed by optical spectroscopy (Figure 4c).^[8] As a matter of fact, it appears that the internal stress/strain state and lattice temperature of the photoexcited film do not trigger further spin-state conversion of SCO molecules on this sub-nanosecond time domain.

3. Conclusion

To summarize, using time-resolved synchrotron X-ray diffraction measurements combined to optical spectroscopy results, we have established the successive dynamical steps of the photoswitching process (from the molecular to the material scale) in nanometric thin films of the SCO compound $[\text{Fe}(\text{HB}(1,2,4\text{-triazol-1-yl})_3)_2]$.

This study enables us to examine the potential interplay that may exist between the structural and electronic dynamical processes in out-of-equilibrium. Advantageously, thin films of **1** prove to be particularly well suited for time-resolved XRD investigations since they exhibit an above-room-temperature spin transition combined to a highly preferred orientation of the nanocrystallites and a sizeable crystal lattice elongation along the orthorhombic c -axis. Several conclusions can be drawn from the present study regarding the photoinduced dynamics of solid-state SCO nanomaterials. First, it suggests the universal existence of a temporal bottleneck in the photo-transformation process of SCO compounds, characterized by sequential dynamics between molecular spin-state switching, on the one hand, and lattice heating and volume expansion, on the other hand. This observation translates into a significant delay between the thermal and mechanical equilibration time of the crystal lattice in nanometric thin films ($\approx 100 \text{ ps}$) and the molecular spin-state switching driven by an Arrhenius-like activation process ($\approx 10 \text{ ns}$). In other words, the equilibration between electronic spin state of molecules and the excited (hot and expanded) lattice only occurs on the tens of nanosecond timescale, while energy dissipation from photoexcited molecules and subsequent lattice volume expansion take place on shorter timescales. The direct consequence is that, on the sub-nanosecond timescale, the lattice volume change occurs in thin films without any modification of the electronic spin state of molecules. Interestingly, these time-separated dynamics are also manifested by the observation of damped acoustic oscillations in the temporal evolution of the crystal lattice expansion, whereas no such oscillations are observed in the fraction of photoswitched molecules. This breathing phenomenon of the nanometric films constitutes a rare observation of acoustic coherence in the out-of-equilibrium dynamics of SCO nano-objects – attesting again the high quality of films of **1**. On the other hand, about ten nanoseconds after laser irradiation, a direct coupling can be observed between lattice volume change and molecular switching upon sufficient excitation density. Both degrees of freedom display joined dynamics, as evidenced by the observation of a

peak (at ≈ 20 – 30 ns) in the temporal evolution of both the c -lattice parameter expansion and the fraction of HS molecules. This result differs from previous studies performed on Fe^{3+} SCO compounds, wherein the volume change upon the SCO remained small so that the experimentally observed lattice expansion was arising mostly from laser induced heating.^[10]

It is important to underline that such a temporal separation between lattice dynamics and electronic spin-state switching should depend on the size of the studied system. For micrometric crystals ($L \approx 100$ μm), the mechanical equilibrium after photoexcitation is expected to be reached at longer timescale, which likely overlaps with the timescale of the thermally activated conversion process, so that volume change and spin-state switching should occur together. An important result, in view of technological applications, is that even if one reduces the size of the system to the nanometric scale, in order to shorten the propagation time of strain waves (and the diffusion time of the heat generated), the electronic state of SCO molecules remains trapped by local energy barriers, delaying any “cooperative” thermo-elastic switching on the nanosecond timescale. On the other hand, this intramolecular energy barrier can be effectively tuned in SCO compounds either by applying an external pressure or by chemical substitution,^[48] which constitutes an interesting scope for future investigations of the dynamical switching processes in molecular thin films of **1**.

4. Experimental Section

Spin-Crossover Samples and Thin Film Preparation: Single crystals and bulk powder of **1** were synthesized in their solvent-free form as described previously.^[19] The films were grown by vacuum thermal evaporation. The bulk powder of the SCO complex was heated at ca. 240 $^{\circ}\text{C}$ in a quartz crucible and evaporated on various substrates (fused silica, single-crystal quartz, and silicon) at a rate of 0.03 \AA s^{-1} at a base pressure of ca. 2×10^{-7} mbar. Film thicknesses were monitored in situ using a quartz crystal microbalance and ex situ by spectral reflectance measurements (Filmetrics, F20). The thickness of the studied films was 175 nm on fused-silica and silicon substrates and 210 nm on quartz substrate. As described previously,^[20] the as-deposited films of **1** were recrystallized by a solvent-vapor annealing treatment, resulting in homogeneous, nanocrystalline thin films, with the orthorhombic c -axis normal to the substrate surface.

Single-Crystal X-Ray Diffraction: Temperature-dependent XRD measurements were performed on a single crystal of **1** using a laboratory SuperNova Agilent Technologies 4-circle diffractometer, with $\text{Cu-K}\alpha$ microsource ($\lambda = 1.5406$ \AA) and EosS2 CCD camera. Using an Oxford Cryosystems 800Plus nitrogen-flow cryostat, the temperature evolution of the unit-cell parameters was measured from 10 to 120 $^{\circ}\text{C}$ with 5 $^{\circ}\text{C}$ intervals, both in heating and cooling mode, with short data collection acquisition at each temperature point. Unit-cell parameters were extracted using the CrysAlisPro software from Rigaku Oxford Diffraction (CrysAlisPro 1.171.39.46 (Rigaku OD, 2018)) during data integration-reduction process.

Synchrotron X-ray Diffraction: XRD experiments on thin films of **1** were performed at the ID09 beamline of the ESRF synchrotron source, in $\frac{1}{2}$ - θ hybrid filling mode. As previously described,^[49] fast rotating choppers were used to isolate X-ray single pulses (each ca. 70 ps long) at 1 kHz repetition rate. The energy of the X-rays was centered at $E = 15$ keV, with a bandwidth $\Delta E/E \approx 1.5\%$. The beam size at sample position was measured as 90 (horizontal) \times 22 (vertical) ± 5 μm . With X-ray incidence angle of 1.5 degree, the X-ray footprint on the sample was ca. 90×900 μm . Diffracted X-rays were integrated on a 2D Rayonix MX170-HS CCD detector. Each diffraction image was recorded with 300 to 1000 shots exposure. The temperature of the film was adjusted using a custom-made ceramic heating plate controlled via a thermocouple probe, which was developed

by the sample environment pool of ESRF. For the time-resolved pump-probe study, a synchronized picosecond laser (Coherent, 800 nm, pulse duration 1.5 ps) was used to excite the sample. The 535 nm excitation wavelength was generated with a TOPAS OPA from LightConversion. The laser beam was shaped using two cylindrical lenses in order to get a footprint at sample position compatible with the X-ray footprint. The size of the laser beam at sample position was ca. 0.3×1.6 mm. The energy density of the pump laser was varied up to a maximum value of 26 mJ cm^{-2} pulse $^{-1}$ (i.e., ≈ 100 μJ per pulse). Measurements were performed in a stroboscopic manner and the time sequence was repeated several times (typ. 5 to 10) in order to increase the statistics. Interleave reference measurements with no laser were recorded in order to correct for the experimental drifts.

Data Reduction and Analysis: pyFAI python library was used to perform the azimuthal averaging on the 2D images and the 1D diffraction patterns. Due to the discrete signatures of the diffraction images (arising from the preferred orientation of the crystallites), the integration range was limited to ± 20 degrees around the selected diffraction peaks. Individual peak fitting was performed using the lmfit python library. A pseudo Voigt function was used to describe the peak shape. The c -lattice parameter was calculated from the refined peak center along the $(00l)$ reciprocal direction ($c = 2\pi/lq$). For the time-resolved data, Δc was calculated as the difference between the value of c obtained at the given time delay and the previous reference measurement with no laser. A custom algorithm allowed to perform averaging over the different repetition of the same time sequence, reject outliers, and calculate the standard deviation in the dataset.

Supporting Information

Supporting Information is available from the Wiley Online Library or from the author.

Acknowledgements

The authors acknowledge the European Synchrotron Radiation Facility (ESRF) for provision of synchrotron radiation facilities under proposal number HC4689. This work received financial support from the Agence Nationale de la Recherche (Project SCOPOL, ANR-22-CE09-0019; Project MULTICROSS, ANR-19-CE29-0018 and Project CRITICLAS, ANR-21-CE30-0011-01). Y.J. acknowledges the financial support from the R&D project “XTRAS” in EuXFEL.

Conflict of Interest

The authors declare no conflict of interest.

Data Availability Statement

The data that support the findings of this study are available from the corresponding author upon reasonable request.

Keywords

lattice dynamics, nanometric films, photoswitching dynamics, spin-crossover materials, time-resolved X-ray diffraction

Received: February 28, 2024

Revised: May 13, 2024

Published online:

[1] C. Thomsen, H. T. Grahn, H. J. Maris, J. Tauc, *Phys. Rev. B* **1986**, *34*, 4129.

- [2] M. Bargheer, N. Zhavoronkov, Y. Gritsai, J. C. Woo, D. S. Kim, M. Woerner, T. Elsaesser, *Science*. **2004**, *306*, 1771.
- [3] D. Schick, M. Herzog, A. Bojahr, W. Leitenberger, A. Hertwig, R. Shayduk, M. Bargheer, *Struct. Dyn.* **2014**, *1*, 064501.
- [4] P. Ruello, V. E. Gusev, *Ultrasonics*. **2015**, *56*, 21.
- [5] C. Mariette, M. Lorenc, H. Cailleau, E. Collet, L. Guérin, A. Volte, E. Trzop, R. Bertoni, X. Dong, B. Lépine, O. Hernandez, E. Janod, L. Cario, V. Ta Phuoc, S. Ohkoshi, H. Tokoro, L. Patthey, A. Babic, I. Usov, D. Ozerov, L. Sala, S. Ebner, P. Böhler, A. Keller, A. Oggenfuss, T. Zmofing, S. Redford, S. Vetter, R. Follath, P. Juranic, et al., *Nat. Commun.* **2021**, *12*, 1239.
- [6] G. de Haan, T. J. van den Hooven, P. C. M. Planken, *Opt. Express*. **2021**, *29*, 32051.
- [7] H. Cailleau, M. Lorenc, L. Guérin, M. Servol, E. Collet, M. Buron-Le Cointe, *Acta Cryst.* **2010**, *A66*, 189.
- [8] K. Ridier, A.-C. Bas, V. Shalabaeva, W. Nicolazzi, L. Salmon, G. Molnár, A. Bousseksou, M. Lorenc, R. Bertoni, E. Collet, H. Cailleau, *Adv. Mater.* **2019**, *31*, 1901361.
- [9] K. Ridier, W. Nicolazzi, L. Salmon, G. Molnár, A. Bousseksou, *Adv. Mater.* **2022**, *34*, 2105468.
- [10] A. Volte, C. Mariette, R. Bertoni, M. Cammarata, X. Dong, E. Trzop, H. Cailleau, E. Collet, M. Levantino, M. Wulff, J. Kubicki, F.-L. Yang, M.-L. Boillot, B. Corraze, L. Stoleriu, C. Enachescu, M. Lorenc, *Commun. Phys.* **2022**, *5*, 168.
- [11] M. Lorenc, J. Hébert, N. Moisan, E. Trzop, M. Servol, M. Buron-Le Cointe, H. Cailleau, M. L. Boillot, E. Pontecorvo, M. Wulff, S. Koshihara, E. Collet, *Phys. Rev. Lett.* **2009**, *103*, 028301.
- [12] R. M. van der Veen, A. Tissot, A. Hauser, A. H. Zewail, *Phys. Chem. Chem. Phys.* **2013**, *15*, 7831.
- [13] R. M. van der Veen, O.-H. Kwon, A. Tissot, A. Hauser, A. H. Zewail, *Nat. Chem.* **2013**, *5*, 395.
- [14] M. Hada, Y. Nishina, T. Kato, *Acc. Chem. Res.* **2021**, *54*, 731.
- [15] P. Gütllich, A. Hauser, H. Spiering, *Angew. Chem., Int. Ed. Engl.* **1994**, *33*, 2024.
- [16] P. Gütllich, H. A. Goodwin, *Spin Crossover in Transition Metal Compounds I-III*, Springer-Verlag, Berlin **2004**.
- [17] A. Bousseksou, G. Molnár, L. Salmon, W. Nicolazzi, *Chem. Soc. Rev.* **2011**, *40*, 3313.
- [18] R. Bertoni, M. Lorenc, H. Cailleau, A. Tissot, J. Laisney, M.-L. Boillot, L. Stoleriu, A. Stancu, C. Enachescu, E. Collet, *Nat. Mater.* **2016**, *15*, 606.
- [19] S. Rat, K. Ridier, L. Vendier, G. Molnár, L. Salmon, A. Bousseksou, *CrystEngComm*. **2017**, *19*, 3271.
- [20] V. Shalabaeva, S. Rat, M. D. Manrique-Juarez, A.-C. Bas, L. Vendier, L. Salmon, G. Molnár, A. Bousseksou, *J. Mater. Chem. C*. **2017**, *5*, 4419.
- [21] A.-C. Bas, V. Shalabaeva, X. Thompson, L. Vendier, L. Salmon, C. Thibault, G. Molnár, L. Routaboul, A. Bousseksou, *C. R. Chim.* **2019**, *22*, 525.
- [22] K. Ridier, A.-C. Bas, Y. Zhang, L. Routaboul, L. Salmon, G. Molnár, C. Bergaud, A. Bousseksou, *Nat. Commun.* **2020**, *11*, 3611.
- [23] R. Bertoni, M. Lorenc, A. Tissot, M. Servol, M.-L. Boillot, E. Collet, *Angew. Chem., Int. Ed.* **2012**, *51*, 7485.
- [24] R. Bertoni, E. Collet, H. Cailleau, M.-L. Boillot, A. Tissot, J. Laisney, C. Enachescu, M. Lorenc, *Phys. Chem. Chem. Phys.* **2019**, *21*, 6606.
- [25] K. Ridier, S. Rat, H. J. Shepherd, L. Salmon, W. Nicolazzi, G. Molnár, A. Bousseksou, *Phys. Rev. B*. **2017**, *96*, 134106.
- [26] P. Guionneau, *Dalton Trans.* **2014**, *43*, 382.
- [27] D. W. Breiby, O. Bunk, J. W. Andreasen, H. T. Lemke, M. M. Nielsen, *J. Appl. Crystallogr.* **2008**, *41*, 262.
- [28] V. Shalabaeva, A.-C. Bas, M. Piedrahita-Bello, K. Ridier, L. Salmon, C. Thibault, W. Nicolazzi, G. Molnár, A. Bousseksou, *Small*. **2019**, *15*, 1903892.
- [29] A. von Reppert, L. Willig, J.-E. Pudell, M. Rössle, W. Leitenberger, M. Herzog, F. Ganss, O. Hellwig, M. Bargheer, *Appl. Phys. Lett.* **2018**, *113*, 123101.
- [30] M. Lorenc, C. Balde, W. Kaszub, A. Tissot, N. Moisan, M. Servol, M. Buron-Le Cointe, H. Cailleau, P. Chasle, P. Czarnecki, M. L. Boillot, E. Collet, *Phys. Rev. B*. **2012**, *85*, 054302.
- [31] W. Gawelda, A. Cannizzo, V.-T. Pham, F. van Mourik, C. Bressler, M. Chergui, *J. Am. Chem. Soc.* **2007**, *129*, 8199.
- [32] C. H. Bressler, C. Milne, V.-T. Pham, A. ElNahhas, R. M. van der Veen, W. Gawelda, S. Johnson, P. Beaud, D. Grolimund, M. Kaiser, C. N. Borca, G. Ingold, R. Abela, M. Chergui, *Science*. **2009**, *323*, 489.
- [33] A. Cannizzo, C. J. Milne, C. Consani, W. Gawelda, C. H. Bressler, F. van Mourik, M. Chergui, *Coord. Chem. Rev.* **2010**, *254*, 2677.
- [34] G. Auböck, M. Chergui, *Nat. Chem.* **2015**, *7*, 629.
- [35] M. M. N. Wolf, R. Groß, C. Schumann, J. A. Wolny, V. Schünemann, A. Døssing, H. Paulsen, J. J. McGarvey, R. Diller, *Phys. Chem. Chem. Phys.* **2008**, *10*, 4264.
- [36] J. Li, R. Clinite, X. Wang, J. Cao, *Phys. Rev. B*. **2009**, *80*, 014304.
- [37] G. Galle, J. Degert, C. Mauriac, C. Etrillard, J. F. Letard, E. Freysz, *Chem. Phys. Lett.* **2010**, *500*, 18.
- [38] G. Gallé, D. Deldicque, J. Degert, T. Forestier, J.-F. Létard, E. Freysz, *Appl. Phys. Lett.* **2010**, *96*, 041907.
- [39] K. Ridier, Y. Zhang, M. Piedrahita-Bello, C. M. Quintero, L. Salmon, G. Molnár, C. Bergaud, A. Bousseksou, *Adv. Mater.* **2020**, *32*, 2000987.
- [40] L. Stoleriu, M. Nishino, S. Miyashita, A. Stancu, R. Bertoni, E. Collet, M. Lorenc, C. Enachescu, *Phys. Rev. B*. **2023**, *108*, 014306.
- [41] M. Mattern, A. von Reppert, S. P. Zeuschner, M. Herzog, J.-E. Pudell, M. Bargheer, *Photoacoustics*. **2023**, *31*, 100503.
- [42] P. Babilotte, P. Ruello, D. Mounier, T. Pezeril, G. Vaudel, M. Edely, J.-M. Breteau, V. Gusev, K. Blary, *Phys. Rev. B*. **2010**, *81*, 245207.
- [43] P. Maity, J. Yin, B. Cheng, J.-H. He, O. M. Bakr, O. F. Mohammed, *J. Phys. Chem. Lett.* **2019**, *10*, 5259.
- [44] J. Wang, J. Zhu, Y. Jiang, M. Li, K. Yu, G. P. Wang, *Nanophotonics*. **2021**, *10*, 4009.
- [45] G. Liang, G. Zhai, J. Ma, H. Wang, J. Zhao, X. Wu, X. Zhang, *J. Phys. Chem. Lett.* **2022**, *13*, 8783.
- [46] M. Harb, W. Peng, G. Sciaini, C. T. Hebeisen, R. Ernstorfer, M. A. Eriksson, M. G. Lagally, S. G. Kruglik, R. J. D. Miller, *Phys. Rev. B*. **2009**, *79*, 094301.
- [47] I. Chaban, R. Deska, G. Privault, E. Trzop, M. Lorenc, S. E. Kooi, K. A. Nelson, M. Samoc, K. Matczyszyn, T. Pezeril, *Nano Lett.* **2022**, *22*, 4362.
- [48] A. Hauser, in *Spin Crossover in Transition Metal Compounds II*, (Eds.: P. Gütllich, H. A. Goodwin), Springer-Verlag, Berlin **2004**, pp. 155–198.
- [49] M. Cammarata, L. Eybert, F. Ewald, W. Reichenbach, M. Wulff, P. Anfinrud, F. Schotte, A. Plech, Q. Kong, M. Lorenc, B. Lindenau, J. Rübiger, S. Polachowski, *Rev. Sci. Instrum.* **2009**, *80*, 015101.